Elimination of spurious modes in full-vectorial finite element method based acoustic modal solution

Aamir Gulistan,[1,*] **M. M. Rahman,**[2] **Souvik Ghosh,**[1] **and B. M. A. Rahman**[1]

[1]*School of Mathematics, Computer Science & Engineering, City, University of London, London EC1V 0HB, UK*

[2]*Department of Electronics and Communications Engineering in East West University, Bangladesh*

[*]*aamir.gulistan@city.ac.uk*

Abstract: Finite element method is a powerful technique for solving a wide range of engineering problems. However, the existence of the spurious solutions in full-vectorial finite element method has been a major problem for both acoustic and optic modal analyses. For emerging photonic devices exploiting light-sound interactions in high index contrast waveguides, this problem is a major limitation. A penalty function is introduced to remove these unwanted spurious modes in acoustic waveguides, which also identifies the acoustic modes more easily. Numerically simulated results also show considerably improved vector mode profiles. The proposed penalty method has been applied for the characterization of low index contrast single mode fiber and also for high index contrast silicon nanowire to demonstrate its effectiveness.

1. Introduction

Stimulated Brillouin Scattering (SBS) is an important nonlinear optical effect that occurs due to the interaction of optical and acoustic waves in a medium. Acoustic waves are generated due to the process of electrostriction where high-intensity light wave traveling through a medium produces mechanical vibrations resulting in the scattered light and phonons [1]. The SBS has attracted considerable attention due to its adverse power limiting effect on the performance of optical networks [2]. Similarly, for high power fiber lasers, which have excellent properties, such as high beam quality, high efficiency, very high output power capability and ease of thermal management, however, the SBS is often considered as one of the main limitations [3]. To overcome this limitation SBS threshold level is required to be increased, which may be achieved by using different techniques, such as the modification of the fiber geometry in order to push the acoustic modes into cladding [4], use a higher effective area multimode fibers [5, 6] or doping fiber with anti-acoustic material to suppress SBS [7]. On the other hand, SBS can be exploited for many useful applications such as temperature and strain sensors. Most recently, the SBS is being exploited for several innovative applications, such as slow and fast light and Brillouin cooling [8–12]. To understand the complex light-sound interactions, accurate analyses of both optical and acoustic modes is required. Various theoretical methods have been reported which can be used for modeling of optical [13] and acoustic [14] waveguides by solving relevant optical and acoustic wave equations [15]. Besides, a commercial solver COMSOL Multiphysics [16] could be used to calculate the Brillouin gain spectrum of optical waveguides.

Full-vectorial finite element (FEM) code can be formulated by considering nodes [17] and edges [18] of a mesh element. FEM based modal solution using node and edge elements are equally efficient and accurate. However, it is observed that the node elements based modal solution contains extraneous nonphysical or spurious modes. A scalar formulation [19, 20] may be a simpler approach and free of spurious solution but the vector formulations are not only

more accurate but also essential, particularly, when optical index contrast is high. In 1984, it was reported that the vector based FEM formulations are affected by the existence of spurious modes [17]. It was identified that as the vector formulation considered only two curl equations but did not consider the divergence-free nature of the field, which allowed spurious modes to appear. As these spurious solutions introduce difficulties to identify physical modes and also deteriorate eigenvector quality, therefore different techniques have been considered to eliminate them.

On the other hand, the classification of acoustic modes is even more complex than that of optical modes. There can be different types of acoustic modes, such as longitudinal, transverse, bending, torsional or flexural modes. For a high index contrast waveguide, these acoustic modes are hybrid in nature. A full-vectorial FEM modal solution provides accurate mode profiles but the existence of the spurious solutions make it challenging to recognize the real modes of interest. Therefore, it is very important to address the appearance of spurious solutions and also to find a way to eliminate them.

In this paper, we used a penalty approach to modify the node element based acoustic wave variational formulation and successfully applied to eliminate the spurious acoustic modes in both low and high index contrast acoustic waveguides. The introduction of penalty term resulted in not only improved quality of acoustic modes but also eliminated spurious modes without deteriorating the eigenvalues of the desired modes. The proposed penalty approach is tested for both low and high index contrast acoustic waveguides, reported in following sections.

2. Spurious modes in optical solutions

The FEM is a powerful and versatile numerical method used for solving the electromagnetic field problems in optical waveguides. The existence of spurious solutions in FEM based vector formulations is often considered as a shortcoming of these formulations. These spurious modes are only numerically generated solutions and have no physical significance and simply considered as wrong solutions [21]. Although the existence of spurious solutions in electromagnetic field problems was identified but little research was carried out in order to eliminate these solutions. Konrad [22] first suggested that rigorous boundary condition can be imposed to eliminate the spurious modes, however, the results were not satisfactory. Rahman and Davies proposed a novel penalty method [17], used with the full-vectorial **H** field formulation to eliminate the spurious modes in the optical modal analysis.

The full-vectorial optical formulation incorporating penalty method based on the minimization of the full **H**-field energy functional [23] is given in Eq. (1).

$$\omega_o^2 = \frac{\int\int[(\nabla\times\mathbf{H})^* \cdot \hat{\varepsilon}^{-1}(\nabla\times\mathbf{H}) + \alpha\,(\nabla\cdot\mathbf{H})^*(\nabla\cdot\mathbf{H})]\,dxdy}{\int\int\mathbf{H}^*\cdot\hat{\mu}\,\mathbf{H}\,dxdy} \tag{1}$$

Here, ω_o is the angular frequency, ω_o^2 is the eigenvalue for the optical system of the equations, **H** is the full-vectorial magnetic field component, * is used for the complex conjugate transpose, $\hat{\mu}$ and $\hat{\varepsilon}$ are the permeability and permittivity tensors, respectively. Here, α is the penalty function weighting factor to impose divergence free magnetic field to eliminate spurious modes.

This approach has been a successful and significant improvement was observed in the quality of optical modes. However, in order to observe the light-sound interaction, the quality of acoustic mode is also very important. In acoustic modal solution, these spurious solutions behave differently and also depends on the type of modes and acoustic index contrast. In order to study acoustic wave propagation in liquid, Winkler and Davies proposed an approach similar to Rahman and Davies, where noticeable reduction of the spurious modes was noted [24]. They proposed to restrict the flexibility of the problem by constraining it. Some improvement in the eigenvectors of the physical modes along the reduction of spurious modes were noted. However, a very small

mesh size, limited to only 24 triangular elements, was considered. Besides that, no study was presented to observe the effect of penalty value on the modes in any acoustic waveguide.

3. Introduction of penalty term in acoustic modal solutions

The acoustic wave propagation along the z-direction is associated with the molecular displacement and for a time harmonic acoustic wave the displacement field, $\mathbf{U_i}$ (in $i=x,\ y\ and\ z$ directions) may be written as in Eq. (2) [25];

$$\mathbf{U_i} = \mathbf{u}(u_x, u_y, ju_z)exp^{j(\omega_a t - k_a z)} \tag{2}$$

Here, ω_a, is the angular acoustic frequency, k_a, is the acoustic propagation constant and u_x, u_y, u_z are particle displacement vectors along the x, y and z directions, respectively. Similarly, the deformation in an acoustically vibrating body is described by the strain field, $\mathbf{S}$, which is related to the partial derivative of the particle displacements, $\mathbf{u}$ and can be written as in Eq. (3) [26];

$$\mathbf{S} = \nabla\mathbf{u} \tag{3}$$

The elastic restoring force can be written in terms of stress field and in a freely vibrating medium the inertial elastic restoring forces are related to translation equation of motion and given as [26, 27];

$$\nabla \cdot \mathbf{T} = \rho\frac{\partial^2\mathbf{u}}{\partial t^2} \tag{4}$$

here, ρ is the material density. Solution of the aforementioned equation depends on the accurate implication of the boundary condition,

$$\mathbf{u} \cdot \hat{n} = 0; \qquad \hat{n} \text{ is the unit vector} \tag{5}$$

and a constraint equation which describes that the rotational energy of the propagating wave is zero.

$$\nabla \times \mathbf{u} = 0 \tag{6}$$

Strain and stress are linearly proportional according to Hooke's Law and can be written as;

$$T_{ij} = c_{ijkl}S_{kl}; \qquad i, j, k, l = x, y, z \tag{7}$$

Here, c_{ijkl} are the microscopic spring constants and termed as elastic stiffness constants. The matrix form of the stiffness tensors can be written as

$$[T] = [c][S] \tag{8}$$

The fundamental FEM based variational expression used in acoustic modal solution can be obtained using strain displacement relation, equation of motion and stress strain relation, as given in Eqs. (3)–(8), and can be written as [24];

$$\omega_a^2 = \frac{\int\int[(\nabla \cdot \mathbf{U})^* \cdot [C](\nabla \cdot \mathbf{U})]\, dxdy}{\int\int \mathbf{U}^* \cdot \rho\mathbf{U}\, dxdy} \tag{9}$$

Here, ω_a is the acoustic angular frequency, $\mathbf{U}$ is the displacement eigenvector, ρ and $[C]$ are the density of the material and elastic stiffness tensor, respectively. The above mentioned acoustic wave equation can be reduced to a general eigenvalue equation [27]:

$$[A]\mathbf{U} - \omega_a^2[B]\mathbf{U} = 0 \tag{10}$$

The [A] matrix is known as the stiffness matrix, related to the strain energy and [B] matrix is the mass matrix related to the kinetic energy. Here, ω_a^2 is the eigenvalue and the eigenvector $\mathbf{U}$ are the unknown values of nodal displacements vectors.

The formulation given by Eq. (9) is considered to be sufficient for modeling of acoustic modes in waveguides. However, this formulation also generates spurious solutions which not only effect the desired mode quality but also introduce difficulty in recognizing the physical modes. To eliminate these spurious modes, Eq. (9) can be modified by adding the two curl equations as a penalty term. The augmented full-vectorial FEM based acoustic formulation is given by Eq. (11). Here, the $\nabla \times \mathbf{U} = 0$ constraint on the displacement vector is introduced in a least squares manner by a weighting factor, the penalty term, α, and this is used to control the elimination of spurious solutions.

$$\omega_a^2 = \frac{\int \int [(\nabla \cdot \mathbf{U})^* \cdot [C](\nabla \cdot \mathbf{U}) + \alpha (\nabla \times \mathbf{U})^* \cdot (\nabla \times \mathbf{U})] \, dxdy}{\int \int \mathbf{U}^* \cdot \rho \, \mathbf{U} \, dxdy} \tag{11}$$

The curl-curl section of the augmented formulation enforces the acoustic field to suppress the rotational energy of the propagating acoustic wave. An increasingly large penalty term makes the Eq. (11) overpower to the shear mode. Therefore, the corresponding eigenvectors move towards the longitudinal mode and results in the spurious free longitudinal modes. This formulation can make a considerable improvement in the acoustic modal solutions by reducing or even eliminating spurious modes along with a significant improvement in the eigenvector quality, as shown in the following sections.

4. Effect of penalty term in low index contrast acoustic waveguide

4.1. Elimination of spurious modes

In order to study the effect of penalty term, first we have considered a low-index contrast single mode optical fiber (SMF) with a core radius of 4.1 μm. The core consist of 6.24 %wt of GeO_2 and 93.76 %wt of SiO_2, whereas, cladding is taken as pure SiO_2. The shear and longitudinal acoustic velocities of the core are taken as as 3644.85 m/s and 5794.626 m/s, respectively. Similarly for cladding, shear and longitudinal velocities are taken as 3760 m/s and 5970 m/s, respectively [28]. The material density of core and cladding are considered as 2291.25 kg/m^3 and 2201 kg/m^3, respectively.

An in-house full-vectorial FEM based computer program for acoustic modal analysis based on the formulation given in Eq. (11) has been developed. We have exploited the available two-fold symmetry and only a quarter of the waveguide is simulated. This allows a much better mesh refinement with given computer resources and also avoid degeneration of modes which have identical eigenvalues [29, 30]. Besides, we have used polar mesh system which is more efficient in the distribution of discretized triangular elements along the curved interface of a circular waveguide [31].

Optical modal analysis has also been carried out for this SMF with the refractive indices of the Ge-doped core and pure silica cladding are taken as 1.44905 and 1.444, respectively at the optical wavelength of 1.55 μm. The propagation constant and effective index of the H_y dominant fundamental optical LP_{01} mode are calculated as $\beta_{op} = 5.86205 \ rad/\mu m$ and $n_{eff} = 1.446116$, respectively, at the operating wavelength of 1.55 μm. However, in order to observe the light-sound interaction in optical waveguides the phase matching condition given in Eq. (12) should also be satisfied [32, 33].

$$k_a = 2 \beta_{opt} \tag{12}$$

Considering the phase matching condition given in Eq. (12) the acoustic propagation constant or wave vector is calculated as k_a=11.7241 $rad/\mu m$. Although, this fiber supports only a single mode for quasi-TE or quasi-TM polarization, however can guide several acoustic modes depending
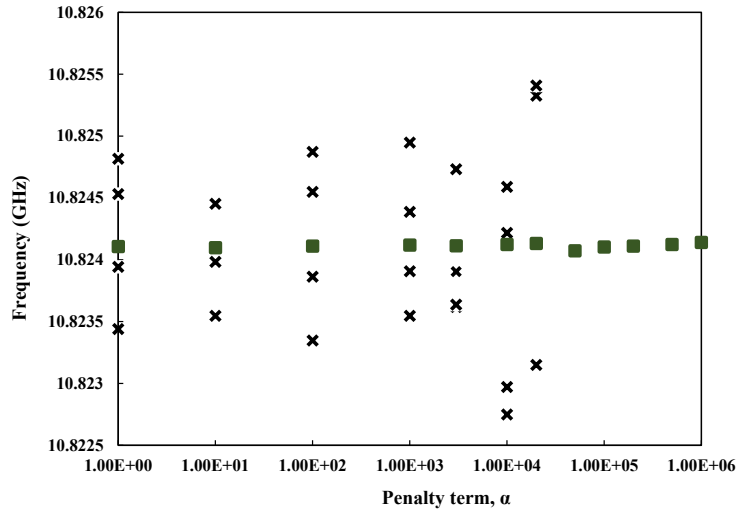
Fig. 1. Reduction of spurious solutions with penalty (α) term for the U_z dominant LP_{01} acoustic mode in a SMF.

on the acoustic wavenumber. The phase matching condition can be fulfilled by multiple acoustic modes having different acoustic velocities and frequencies. This results in the interaction of the LP_{01} optical mode with not only the fundamental acoustic mode but also with other higher order acoustic modes. The phase-matched fundamental longitudinal acoustic (LP_{01}) mode with dominant U_z vector is found at frequency 10.82414 GHz with its corresponding acoustic velocity of 5800.8391 m/s. However, when a computer code using Eq. (9) is considered, in addition to this fundamental longitudinal acoustic mode, unfortunately, many other non-physical modes were also observed in the modal solutions. The existence of these spurious modes resulted in difficulty to identify a particular mode of interest and multiple iterations were carried out in order to find the correct mode. In addition to this, the original mode quality was also significantly affected by the existence of spurious modes when no penalty term is used. Figure 1 shows the presence of a single physical LP_{01} mode shown by a square and many other non-physical spurious modes by crosses, respectively, with the increase in the penalty value (α). In each simulation run maximum five eigenvalues were obtained. It can be observed that when $\alpha = 0$, there are four spurious modes (shown by crosses) in the vicinity along with only one physical mode (green square), which is the fundamental longitudinal (LP_{01}) acoustic mode in this case. However, when the value of α is more than 1×10^5, the spurious modes vanish completely and the mode quality also improves significantly. Moreover, it can also be observed that the frequency of fundamental longitudinal mode at $\alpha = 1 \times 10^5$ remains almost the same as that is obtained when $\alpha = 0$. Effect of penalty value on the eigenvalue accuracy is discussed later.

4.2.   Improvement in the mode quality

Figure 2 shows the dominant and non-dominant vector displacement profiles of the fundamental longitudinal acoustic LP_{01} mode when no penalty term was used ($\alpha = 0$). The dominant U_z displacement vector of the LP_{01} mode is only slightly affected by the presence of spurious solutions, as shown in Fig. 2(c), but where a closer inspection shows small ripples in the contour lines. However, the non-dominant displacement vectors U_x and U_y profiles shown in Figs. 2(a) and 2(b), respectively, are more noisy than the dominant U_z vector profile. As in this case, the magnitude of non-dominant displacement vectors U_x and U_y were 40 times smaller than that of the dominant U_z vector, so the smaller non-dominant displacement vectors were more affected

by the noise and are of significantly poor quality. Maybe because of such poor quality, nature of non-dominant displacement vectors of acoustic modes has often not been discussed in published reports. As the available two-fold symmetry of the fiber is exploited here, so only a quarter of the structure is shown in Fig. 2. The Gaussian-like displacement vector profile of the dominant U_z vector has the peak value at the center of the core and monotonically decreases along the radius of the fiber. However, the non-dominant U_x displacement vector has maxima on the x-axis and zero value along the y-axis as shown in Fig. 2(a). Similarly, the non-dominant U_y displacement vector has maxima value along the y-axis and zero along the x-axis as shown in Fig. 2(b). However, quality of these non-dominant components shown here is very poor.
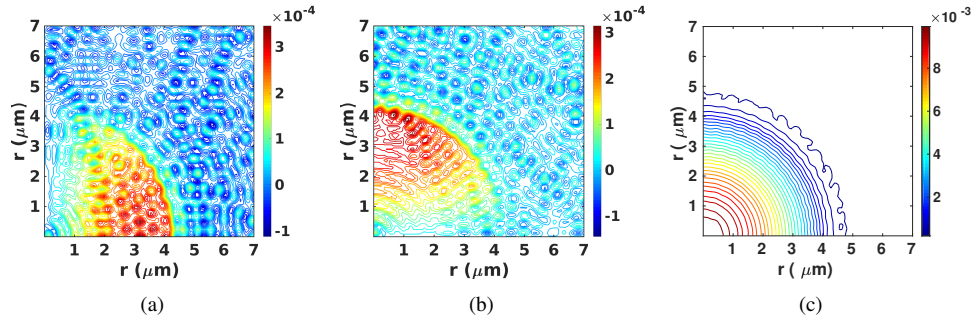

Fig. 2. Dominant and non-dominant displacement vector profiles of the fundamental longitudinal LP_{01} acoustic mode for $\alpha = 0$ where, (a) U_x, (b) U_y and (c) U_z contours, respectively.

The possible reason for noise in the vector displacement profiles of longitudinal acoustic modes is that, for a lower or zero value of α, the spurious modes with eigenvalues close to the desired physical modes, which in this case is the LP_{01} mode, perturbed this truly physical mode. When two eigenvalues are close then their eigenvectors can easily get mixed up during eigenvalue solutions. However, after the introduction of the penalty term and choosing $\alpha = 1 \times 10^5$, the eigenvalues of spurious modes are pushed away from the physical mode and results in a clean mode profile, as shown in Fig. 3.
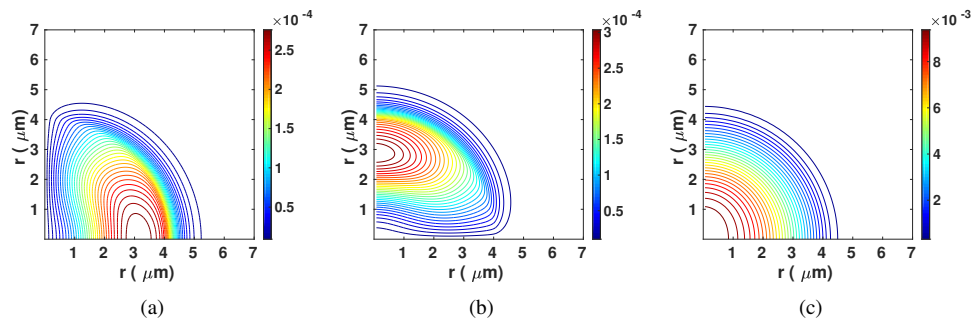

Fig. 3. Dominant and non-dominant displacement vector profiles of the fundamental longitudinal LP_{01} acoustic mode for $\alpha = 10^5$, where, (a) U_x, (b) U_y and (c) U_z contours, respectively.

It can be observed that the non-dominant U_x and U_y displacement vectors of LP_{01} acoustic mode shown in Figs. 3(a) and 3(b), respectively, have significantly improved compared to the mode profiles shown earlier in Fig. 2, without the use of a penalty term. This significant

improvement in the mode quality not only provides a more accurate modal solution but also allows us to understand the full-vectorial nature of these modes, their profiles and relative magnitudes and if possible to exploit them. It also helps to utilize computer resources more efficiently by reducing the multiple iterations often needed to refine individual modes.
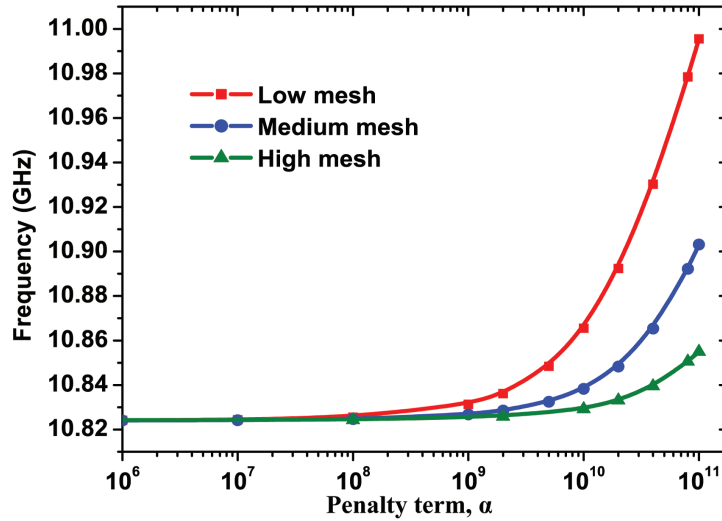

Fig. 4. Variation of frequency with respect to change in the value of penalty term (α) for the U_z dominant LP_{01} acoustic mode.

4.3. Effect of penalty and mesh density on modal solution

It is well known that the solution accuracy of FEM based modal solution is strongly dependent on the discretized mesh elements. Hence, in our simulations, polar mesh is used and mesh density was varied with different values of α. For our analyses we have used three different mesh densities as low, medium, and high with 119800, 479600, and 1439400 first-order triangular elements, respectively, to see the impact on the frequency shift with the penalty factor. The frequency of the fundamental longitudinal mode is calculated as 10.823981 GHz, 10.824098 GHz, and 10.829219 GHz for a low, medium and high mesh densities, respectively, at $\alpha = 10^5$. Although, the variation in the frequency is little, however, we have used a moderate value of α to avoid spurious modes along with a finer mesh for our subsequent simulations to achieve a higher accuracy.

Figure 4 shows the effect on frequency when the penalty term, α increases from 1×10^6 to a very higher value in the order of 1×10^{11}. It can be noted that the frequency did not change significantly up to 1×10^6 and so not shown here. However, when the penalty factor is increased more to observe its behavior on the frequency, it can be noticed that the acoustic frequency increases. This increase in frequency is also strongly related to the density of mesh distribution used. When a more dense mesh is used, the increase is less as compared to a relatively coarse mesh division. This is due to the fact that higher mesh distribution is more accurate than the lower mesh. For this reason, we have used a much refined mesh distribution for our modal solutions to achieve a higher accuracy.

4.4. Effect of penalty term on higher order longitudinal modes

As mentioned earlier that for a given optical mode, the phase matching condition given by Eq. (12) may be satisfied by multiple acoustic modes. Which suggest that several acoustic modes can

interact with the fundamental optical mode in a SMF and hence it is also necessary to study these higher order acoustic modes. To observe the impact of penalty term we have also simulated some higher order acoustic modes and the results clearly demonstrate highly improved eigenvectors similar to that of the fundamental acoustic mode, shown earlier in Fig. 3.
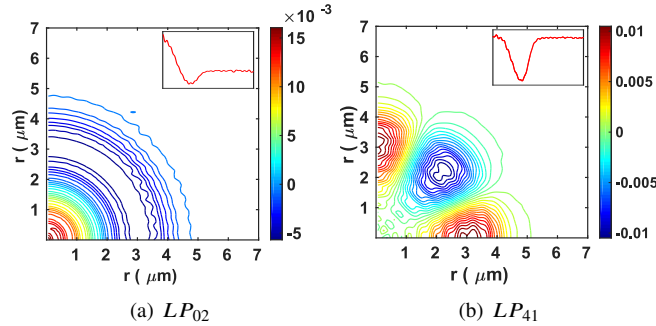

(a) LP_{02} (b) LP_{41}

Fig. 5. Dominant U_z displacement vector contours of higher order longitudinal acoustic modes for $\alpha = 0$.
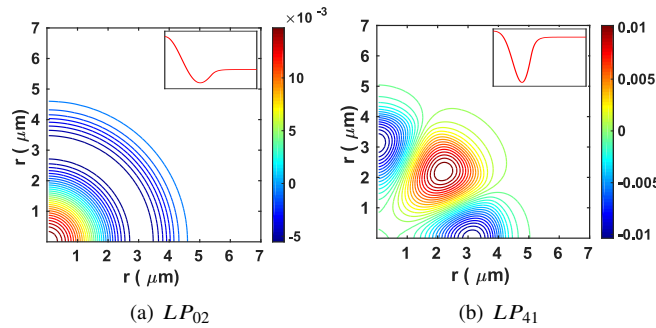

(a) LP_{02} (b) LP_{41}

Fig. 6. Dominant U_z displacement vector contours of higher order longitudinal acoustic modes for $\alpha = 10^5$.

Figures 5(a) and 5(b) show the dominant U_z vector profiles of two higher order LP_{02} and LP_{41} longitudinal acoustic modes, respectively for $\alpha = 0$. Variation of displacement vector profile of these modes along the fiber radius are also shown as insets. The ripples in contour plots of the displacement vector clearly show that the higher order mode profiles are also considerably affected by the presence of spurious modes. It can be noted that, even quality of this dominant component of higher order mode is poor compared that of the fundamental LP_{01} acoustic mode, shown in Fig. 2(c). The quality of their non-dominant displacement vector profiles was even worse than that of LP_{01} acoustic mode and not shown here. However, the introduction of penalty term in acoustic formulation resulted in much smooth contour plots of these two higher order LP_{02} and LP_{41} acoustic modes and these are as shown in Fig. 6. Variations of their displacement vectors along the radius of the fiber are also shown as the insets in Fig. 6.

Table 1 shows the frequency shift and longitudinal velocities of fundamental and higher order longitudinal modes for $\alpha = 0$ and $\alpha = 10^5$. It can be observed that there is only a small change in these values which indicate the accuracy of the modal solutions are not affected when the penalty terms are used.

Table 1. Effect of α on frequency shift and longitudinal velocities of the fundamental and higher order longitudinal acoustic modes.

Mode	Without penalty (α=0)		With Penalty (α=10^5)	
	Frequency shift (GHz)	Longitudinal velocity (m/s)	Frequency shift (GHz)	Longitudinal velocity (m/s)
LP_{01}	10.8241	5800.8391	10.8240	5800.8257
LP_{02}	10.8732	5827.1568	10.8730	5827.059
LP_{41}	10.9265	5855.7582	10.9275	5856.277
LP_{03}	10.9593	5873.2883	10.9591	5873.1817

5. Effect of penalty term in high index contrast acoustic waveguide

Recently, SBS based nanowire structures are also being considered for many exotic photonic devices, such as microwave photonic filters [34], resonators [35] and on-chip high-performance optical signal processing [36, 37]. Acoustic modes in high index contrast acoustic waveguides are even more complex than in a low index contrast optical fiber. The magnitudes of their non-dominant displacement vectors are higher and displacement vector profiles often have stronger spatial variations. In order to observe the effect of penalty term in such nano-structures,
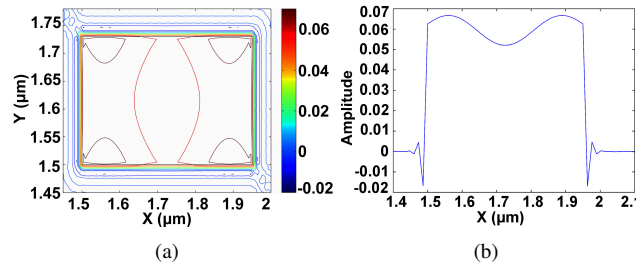

(a)   (b)

Fig. 7. (a) The dominant U_z vector displacement of a highly hybrid mode and (b) is the variation along the x-axis, when $\alpha = 0$.

(a)   (b)   (c)

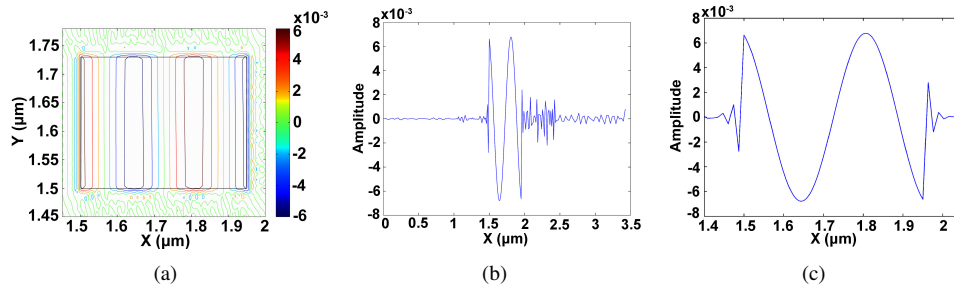Fig. 8. (a) The non-dominant U_x vector displacement profile of a highly hybrid longitudinal mode (b) the variation of U_x displacement vector along the x-axis when $\alpha = 0$, and (c) when $\alpha = 100$.

next, we have considered a high index contrast air-clad silicon nanowire for modal solutions. Here, we have considered a suspended silicon nanowire with its width and height being 450 nm

and 230 nm, respectively. The acoustic shear and longitudinal velocities of silicon are taken as $V_s = 5840 \ m/s$, $V_l = 8433 \ m/s$, respectively. Similarly, the longitudinal velocity of air is chosen as 340 m/s while the shear velocity is zero. The material densities of silicon and air are taken as ρ_{si}=2331 kg/m^3 and ρ_{air}=1.29 kg/m^3, respectively. Moreover, the phase matched acoustic propagation constant is calculated as $k_a = 18.47796 \ rad/\mu m$.

The contour plot of the dominant U_z displacement vector of a highly hybrid mode at $f = 24.8012$ GHz and $V = 8433.3184 \ m/s$, is shown in Fig. 7(a). The dominant U_z displacement vector profile of this longitudinal acoustic mode has a reasonably clean profile without the penalty term. However, still poor quality contour lines can be clearly observed just outside the core as shown in Fig. 7(a). From the dominant U_z vector displacement profile along the x-axis, shown in Fig. 7(b), it can be observed that the amplitude nearly constant inside core but with a superimposed sinusoidal like variation and reduces rapidly to zero value with damping oscillations at the core and cladding interfaces.

However, the non-dominant U_x and U_y vector displacement profiles with their small magnitudes are more susceptible to the existence of the spurious modes. Figure 8(a) shows the contour plot of the non-dominant U_x vector displacement profile of this highly hybrid mode without the use of a penalty term. The non-dominant U_x vector has almost constant magnitude along the y-axis, but with two positive and two negative peaks along the x-axis. Its variation along the x-axis is shown in Fig. 8(b). Two positive and two negative peaks are visible but very noisy oscillations outside the core is also clearly visible in Fig. 8(b) when no penalty term is used. However, with the introduction of penalty value ($\alpha = 100$), the vector displacement profiles is improved significantly and damped oscillations at the two interfaces are clearly visible, as shown in Fig. 8(c). It can also be noted that for this high-index contrast waveguide, non-dominant vectors are relatively large (here $1/10^{th}$) compared to a low index contrast SMF ($1/40^{th}$ only), shown earlier. It should be noted that non-dominant displacement vectors of a high index contrast acoustic waveguide are high and a full-vectorial acoustic analysis should be necessary.

The penalty term is mainly used to eliminate the spurious solutions and to improve the accuracy of the acoustic modal solution. Hence, it has very little effect on the acoustic mode's frequency and velocity of propagation. The optimum value of the penalty term for both low and high index contrast waveguides is obtained by 'trial and error' method. The value is increased from zero to a higher value in both low and high index contrast waveguides until all spurious modes are removed. It is observed that for a low index contrast waveguides the penalty value needs to be higher such as $\alpha = 10^5$ and for low index contrast a low value of $\alpha = 100$ is sufficient to eliminate the spurious modes.

6. Conclusion

A new full-vectorial finite element method based formulation is proposed here to suppress spurious modes for both low index and high index contrast acoustic waveguides. The FEM based vector formulation is not only more accurate but essential to study high index contrast waveguides. However, the existence of spurious solutions often deteriorates the quality of a physical mode. A penalty function, incorporating curl equation is used in order to eliminate these unwanted spurious modes. Effect of full-vectorial nature of the acoustic modes can only be studied through accurate characterization of the dominant and non-dominant displacement vector profiles. Our proposed method clearly demonstrated the significant improvement in the quality of the mode profiles. The spurious modes have been totally removed for low index contrast SMF and also for high index contrast waveguides. Our proposed penalty method results in improving the mode quality which will be useful to study complex light-sound interaction by employing the full-vectorial mode profiles in optical waveguides for many potential applications and optimize their performances.

References

1. A. Yeniay, J. M. Delavaux, and J. Toulouse, "Spontaneous and stimulated Brillouin scattering gain spectra in optical fibers," J. Lightwave Technol. **20**(8), 1425 (2002).
2. H. L. Bras, M. Moignard, and B. Charbonnier, "Brillouin scattering in radio over fiber transmission," in National Fiber Optic Engineers Conference, OSA Technical Digest Series (Optical Society of America, 20017), paper JWA86.
3. J. Limpert, F. Roser, S. Klingebiel, T. Schreiber, C. Wirth, T. Peschel, R. Eberhardt, and A. Tunnermann, "The rising power of fiber lasers and amplifiers," IEEE J. Sel. Top. Quantum Electron. **13**(3), 537–545 (2007).
4. M. J. Li, X. Chen, J. Wang, A. B. Ruffin, D. T. Walton, S. Li, D. A. Nolan, S. Gray, and L. A. Zenteno, "Fiber designs for reducing stimulated Brillouin scattering," in Optical Fiber Communication Conference (Optical Society of America, 2006), p. 3.
5. S. Ramachandran, J. M. Fini, M. Mermelstein, J. W. Nicholson, S. Ghalmi, and M. F. Yan, "Ultra large effective area, higher order mode fibers: a new strategy for high power lasers," Laser Photonics Rev. **2**(6),429–448 (2008).
6. M. D. Mermelstein, S. Ramachandran, J. M. Fini, and S. Ghalmi, "SBS gain efficiency measurements and modeling in a 1714 μm^2 effective area LP_{08} higher-order mode optical fiber," Opt. Express **15**(24), 15952–15963 (2007).
7. S. Gray, D. T. Walton, X. Chen, J. Wang, M-J. Li, A. Liu, A. B. Ruffin, J. A. Demeritt, and L. A. Zenteno, "Optical fibers with tailored acoustic speed profiles for suppressing stimulated Brillouin scattering in high-power, single-frequency sources," IEEE J. Sel. Top. Quantum Electron. **15**(1), 37–46 (2009).
8. M. A. Soto, G. Bolognini, and F. Di Pasquale, "Enhanced simultaneous distributed strain and temperature fiber sensor employing spontaneous Brillouin scattering and optical pulse coding," IEEE Photonics Technol. Lett. **21**(7), 450–452 (2009).
9. L. Thevenaz, M. Nikles, A. Fellay, M. Facchini, and P. Robert, "Truly distributed strain and temperature sensing using embedded optical fibers," Proc. SPIE 3330, 301–314 (1998).
10. K. Y. Song, K. S. Abedin, K. Hotate, M. G. Herraez, and L. Thevenaz, "Highly efficient Brillouin slow and fast light using As_2Se_3 chalcogenide fiber," Opt. Express **14**(13), 5860–5865 (2006).
11. T. Schneider, "Time delay limits of stimulated-Brillouin-scattering-based slow light systems," Opt. Lett. **33**(13), 1398–1400 (2008).
12. G. Bahl, M. Tomes, F. Marquardt, and T. Carmon, "Observation of spontaneous Brillouin cooling," Nat. Phys. **8**(3), 203–207 (2012).
13. S. Selleri, L. Vincetti, A. Cucinotta, and M. Zoboli, "Complex FEM modal solver of optical waveguides with PML boundary conditions," Opt. Quantum Electron. **33**(4), 359–371 (2001).
14. W. W. Zou, Z. Y. He, and K. Hotate,"Two-dimensional finite element modal analysis of Brillouin gain spectra in optical fibers," IEEE Photon. Technol. Lett. **18**(23), 2487–2489 (2006).
15. C. Wolff, M. J. Steel, B. J. Eggleton, and C. G. Poulton, "Stimulated Brillouin scattering in integrated photonic waveguides: Forces, scattering mechanisms, and coupled-mode analysis," Phys. Rev. A. **92**(1), 013836 (2015).
16. S. Dasgupta, F. Poletti, S. Liu, P. Petropoulos, D. J. Richardson, L. Gruner-Nielsen, and S. Herstrom, "Modeling Brillouin gain spectrum of solid and microstructured optical fibers using a finite element method," J. Lightwave Technol. **29**(1), 22–30 (2011).
17. B. M. A. Rahman and J. B. Davies, "Penalty function improvement of waveguide solution by finite elements," IEEE Trans. Microw. Theory Tech. **32**(8), 922–928 (1984).
18. M. Koshiba, "Optical waveguide theory by the finite element method," IEICE Trans. Electronics **97**(7), 625–635 (2014).
19. W. Zou, Z. He, and K. Hotate, "Acoustic modal analysis and control in W-shaped triple-layer optical fibers with highly-germanium-doped core and F-doped inner cladding," Opt. Express **16**(14), 10006–10017 (2008).
20. Y. S. Mamdem, E. Burov, L. A. de Montmorillon, Y. Jaouen, G. Moreau, R. Gabet, and F. Taillade, "Importance of residual stresses in the Brillouin gain spectrum of single mode optical fibers," Opt. Express **20**(2), 1790–1797 (2012).
21. D. Sun, J. Manges, X. Yuan, and Z. Cendes, "Spurious modes in finite-element methods," IEEE Antennas Propag. Mag. **37**(5), 12–24 (1995).
22. A. Konrad, "Vector variational formulation of electromagnetic fields in anisotropic media," IEEE Trans. Microw. Theory Tech. **24**(9), 55–559 (1976).
23. B. M. A. Rahman and A. Agrawal, *Finite Element Modeling Methods for Photonics* (Artech House, 2013).
24. J. R. Winkler and J. B. Davies, "Elimination of spurious modes in finite element analysis," J. Comput. Phys. **56**(1), 1–14 (1984).
25. P. E. Lagasse, "Higher–order finite–element analysis of topographic guides supporting elastic surface waves," J. Acoust. Soc. Am. **53**(4), 1116–1122, (1973).
26. B. A. Auld, *Acoustic Fields and Waves in Solids*, Vol. 2 (Ripol Classic, 1973).
27. S. Sriratanavaree, B. M. A. Rahman, D. M. H. Leung, N. Kejalakshmy, and K. T. V. Grattan, "Rigorous characterization of acoustic-optical interactions in silicon slot waveguides by full-vectorial finite element method," Opt. Express **22**(8), 9528–9537 (2014).
28. I. C. M. Littler, L. B. Fu, E. C. Magi, D. Pudo, and B. J. Eggleton, "Widely tunable, acousto-optic resonances in chalcogenide As_2Se_3 fiber," Opt. Express **14**(18), 8088–8095 (2006).
29. S. Virally, N. Godbout, S. Lacroix, and L. Labonte, "Two-fold symmetric geometries for tailored phasematching in birefringent solid-core air-silica microstructured fibers," Opt. Express **18**(10), 10731–10741 (2010).
30. M. Koshiba and K. Inoue, "Simple and efficient finite–element analysis of microwave and optical waveguides," IEEE

Trans. Microw. Theory Tech. **40**(2), 371–377 (1992).

31. A. Kumar, V. Rastogi, A. Agrawal, and B. M. A. Rahman, "Birefringence analysis of segmented cladding fiber," Appl. Opt. **51**(15), 3104–3108, (2012).

32. P. Dainese, P. S. J. Russell, N. Joly, N., J. C. Knight, G. S. Wiederhecker, H. L. Fragnito, V. Laude, and A. Khelif, "Stimulated Brillouin scattering from multi-GHz-guided acoustic phonons in nanostructured photonic crystal fibres," Nat. Phys. **2**(6), 388 (2006).

33. A. Gulistan, M. M. Rahman, S. Ghosh, and B. M. A. Rahman, "Tailoring light-sound interactions in a single mode fiber for the high-power transmission or sensing applications," Proc. SPIE **10714**, 1071403 (2018).

34. A. C. Bedoya, B. Morrison, M. Pagani, D.Marpaung, and B. J. Eggleton, "Tunable narrowband microwave photonic filter created by stimulated Brillouin scattering from a silicon nanowire," Opt. Lett. **40**(17), 4154–4157 (2015).

35. R. Zhang, J. Sun, G. Chen, M. Cheng, and J. Jiang, "Demonstration of highly efficient forward stimulated Brillouin scattering in partly suspended silicon nanowire racetrack resonators," Appl. Phys. Lett. **111**(3), 031102 (2017).

36. R. Pant, C. G. Poulton, D. Y. Choi, H. Mcfarlane, S. Hile, E. Li, L. Thevenaz, B. L. Davies, S. J. Madden, and B. J. Eggleton, "On-chip stimulated Brillouin scattering," Opt. Express **19**(9), 8285–8290 (2011).

37. M. S. Kang, A. Butsch, and P. St. J. Russell, "Reconfigurable light-driven opto-acoustic isolators in photonic crystal fiber," Nat. Photonics **5**(9), 549–553 (2011).